Hyunho Shin[1]
Mechanics of Materials and Design Laboratory,
Department of Materials Engineering,
Gangneung-Wonju National University,
Gangneung, Gangwon-do 25457, South Korea
e-mail: hshin@gwnu.ac.kr

Jae-Ha Lee
Mechanics of Materials and Design Laboratory,
Department of Materials Engineering,
Gangneung-Wonju National University,
Gangneung, Gangwon-do 25457, South Korea
e-mail: jh_lee@gwnu.ac.kr

Jong-Bong Kim[1]
Department of Mechanical and Automotive Engineering,
Seoul National University of Science and Technology,
Nowon-gu, Seoul 01811, South Korea
e-mail: jbkim@seoultech.ac.kr

Seung-Jae Seo
Poongsan Inc.,
Angang, Gyeongbuk 38026, South Korea
e-mail: topgun2010@poongsan.co.kr

Jaekun Lee
Poongsan Inc.,
Angang, Gyeongbuk 38026, South Korea
e-mail: jae-kun.lee@poongsan.co.kr

Jong-Oek Lee
Poongsan Inc.,
Angang, Gyeongbuk 38026, South Korea
e-mail: leejong@poongsan.co.kr

Tae-Sik Yoon
Defense Industry Technology Center,
Yongsan-gu, Seoul 04353, South Korea;
Defense Acquisition Program,
Kwangwoon University,
Nowon-gu, Seoul 01897, South Korea
e-mail: yuntae76@add.re.kr

Chanseok Jeong
Defense Industry Technology Center,
Yongsan-gu, Seoul 04353, South Korea
e-mail: csjeong203@daum.net

Numerical Verification of the Schroeder–Webster Surface Types and Friction Compensation Models for a Metallic Specimen in Axisymmetric Compression Test

Three types of surfaces in the Schroeder–Webster (SW) theory, i.e., sliding, mixed, and sticking surfaces, have been verified via finite element analysis of an axisymmetric compression test for a metallic specimen. Judging from (i) the radial profile of the pressure at the top elements and (ii) the radial displacement at the top nodes, the three types of SW surfaces are not manifested in the numerical simulation. However, the SW friction compensation model developed for the SW-sliding surface is remarkably reliable in predicting the measured stress–strain curve of the barreled specimen down to the height-to-diameter ratio of 0.1. The origin of this reliability is discussed along with recommendations for using the SW friction compensation model for the SW-sliding surface. [DOI: 10.1115/1.4044131]

Keywords: friction compensation model, contact surface, pressure profile, Schroeder–Webster theory

1 Introduction

Precise calibration of a constitutive equation [1–3] is required to simulate the mechanical deformation behavior of materials and structures accurately. A stress–strain curve measured under a friction-free condition resulting in uniform deformation in a homogeneous stress state is required to calibrate a constitutive equation. Compression testing of an axisymmetric specimen would be one of the handiest methods for obtaining the stress–strain curve. However, it is not easy to determine the friction-free stress–strain curve of materials in a compression test. For instance, a plastically deforming metallic material usually undergoes barreling (nonuniform deformation) under compression owing to friction, which leads to overestimation of the stress–strain curve. Therefore, the effects of friction, lubrication, and barreling on the measured compressive stress–strain curve of metallic specimens have received considerable research attention [4–17].

In the compression test, the influence of friction increases as the height-to-diameter ratio (H/D) of the specimen decreases. Therefore, for a metallic specimen, a higher H/D ratio is desirable, provided the phenomenon of buckling can be avoided; the H/D ratio of approximately 1.5–2.0 is generally employed to obtain a nearly friction-free stress–strain curve. However, in some cases, the H/D ratio of the specimen is inevitably lower than 1.0, e.g., thin plate specimens in a quasistatic test. In high-strain-rate tests such as the split Hopkinson bar test [18], direct impact test [19], and plate impact test [20], a thin specimen has an advantage in achieving a high strain rate. In this

[1]Corresponding authors.

Contributed by the Tribology Division of ASME for publication in the JOURNAL OF TRIBOLOGY. Manuscript received July 21, 2018; final manuscript received June 20, 2019; published online July 17, 2019. Assoc. Editor: Sinan Muftu.

regard, it is necessary to compensate the influence of friction on the measured stress–strain curve obtained in both quasistatic [21–38] and dynamic compressive tests [18–20,39–48].

This study aims to obtain a friction-free stress–strain curve of a metallic material from a curve measured under a frictional condition in an axisymmetric compression test. The geometry of the specimen considered in this study is illustrated in Fig. 1(*a*). For obtaining the friction-free stress–strain curve, a friction compensation model, $f(\mu, H/D)$, is necessary, which describes the ratio of the measured flow stress (p_a) to the friction-free flow stress (σ_o): $p_a/\sigma_o = f(\mu, H/D)$. Once $f(\mu, H/D)$ is known, σ_o can be obtained from the measured flow stress under a frictional condition (p_a). The determined σ_o in this way can be used to calibrate a constitutive equation and to calculate the required load for metal forming and forging.

According to the study of Schroeder and Webster (SW) [21], there are certain conditions (in terms of μ and H/D) in the axisymmetric compression test of a metallic specimen under which (i) the entire contact surface is sliding, (ii) the inner part of the contact surface is sticking while the outer annular part is sliding, or (iii) the entire contact surface is sticking. They derived friction compensation models for each type of contact surface. As for the first case where the entire contact surface is sliding, in addition to the two aforementioned scholars, numerous researchers provided their own friction compensation models, which will be described in Sec. 2.2.

All the friction compensation models available in the literature were derived based on the common assumptions that (i) there is no barreling of the specimen and (ii) inclusion of the frictional force does not alter the stress state of the specimen [27]. Therefore, as the axial strain increases, the applicability of the compensation models is limited because barreling/rollover of the side wall generally occurs in the compression test. Their applicability is also limited when the H/D ratio of the specimen is small because the effect of inclusion of the shear force increases as the thickness of the specimen decreases.

In the literature, researchers used compensation models of their own choice (as will be discussed in Sec. 2.2) to compensate their experimentally obtained stress–strain curves. In this regard, if the reliability of the compensation models derived under the above-mentioned common assumptions is examined for ranges of H/D and μ values, the result may be helpful to researchers attempting to select an appropriate friction compensation model.

In this study, after reviewing the SW theory and the friction compensation models, the three types of surfaces in the SW theory are verified numerically. Subsequently, the reliability of the compensation models available in the literature (including the ones proposed by Schroeder and Webster) is numerically examined to provide researchers a selection guide for an appropriate friction compensation model in an axisymmetric compression test.

2 Review of Schroeder–Webster Theory and Compensation Models

2.1 Schroeder–Webster Theory

2.1.1 Sliding Surface. To describe the behavior of a *sliding* surface, Schroeder and Webster [21] employed the law of Coulomb friction (Fig. 1(*b*))

$$\tau = \mu p \tag{1}$$

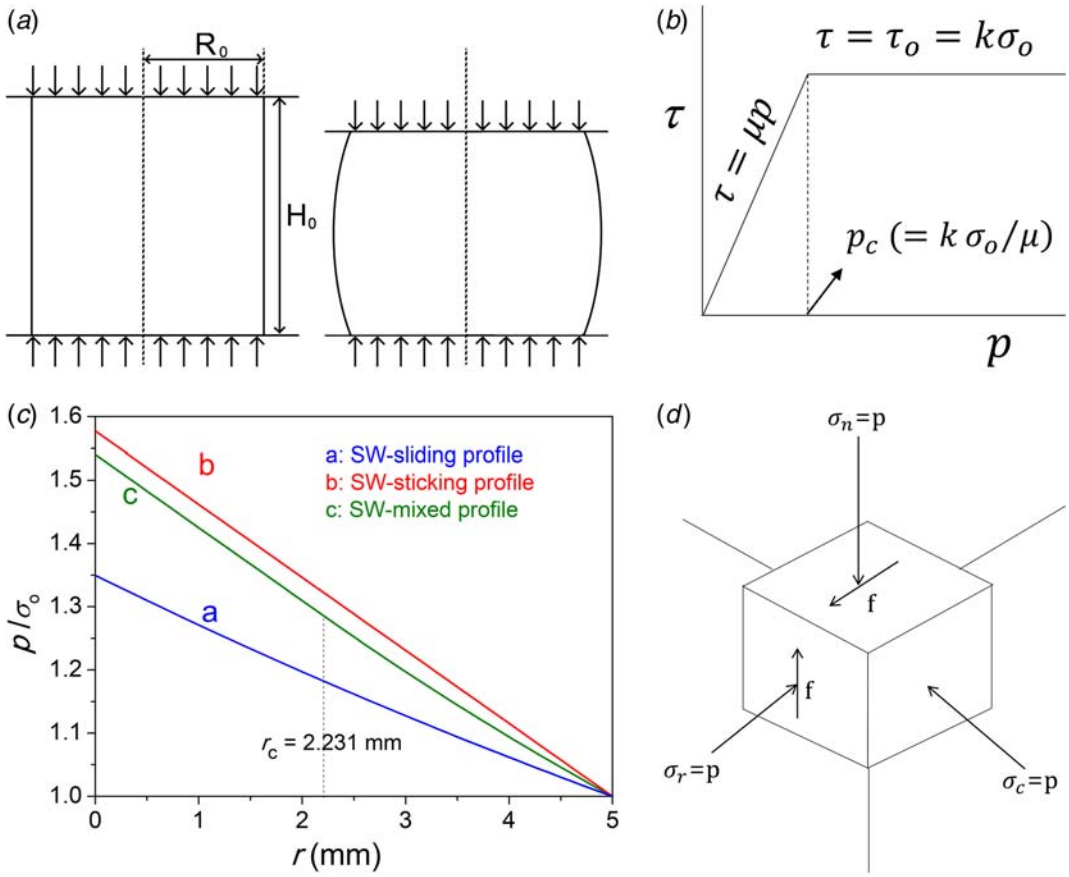

Fig. 1 (*a*) Geometry of the specimen considered in this study for the axisymmetric compression test. (*b*) Laws of Coulomb friction and constant friction. (c) Profile of the pressure for the case when $R = 5$ mm and $H = 10$ mm ($\mu = 0.3$, 0.45, and 0.6 for the SW-sliding, SW-mixed, and SW-sticking profiles, respectively.). (*d*) Stress state when the frictional stress τ is superimposed to a hydrostatic pressure state.

They used Eq. (1) considering the stress equilibrium of an axisymmetric stress element being compressed and established a differential equation

$$\frac{dp}{p} = -\frac{2\mu}{H}dr \tag{2}$$

By integrating Eq. (2) from σ_o to p (the left side) and from R to r (the right side), the profile of the pressure p was obtained as a function of the radial position (r)

$$p = \sigma_o \exp\left[\frac{2\mu}{H}(R-r)\right] \tag{3}$$

Equation (3) is called the "SW-sliding pressure profile" in this study. An example of this profile is illustrated in Fig. 1(*c*) as curve "a".

The average value of the pressure (p_a) can be calculated from the pressure profile (p) as shown in Fig. 1(*a*) (curve "a"), using the equation

$$p_a = \frac{\int_0^R 2\pi r p dr}{\pi R^2} \tag{4}$$

In the experiment, the value of p_a is measured. By substituting Eq. (3) into Eq. (4), the friction compensation model is obtained as

$$\frac{p_a}{\sigma_o} = \frac{2}{\alpha^2}[e^\alpha - \alpha - 1] \tag{5}$$

where $\alpha = \mu D/H$. In this study, Eq. (5) is called the "SW-sliding compensation model." As mentioned, when the friction-free property σ_o is obtained from the measured value of p_a under the frictional condition, equations such as Eq. (5) are called friction compensation models. If the load required for upsetting (p_aA) is predicted from the value of σ_o, equations such as Eq. (5) are called the prediction models for the upsetting load.

2.1.2 Sticking Surface. The term *sticking* used in the SW theory does not necessarily indicate adhesion at the interface; it indicates the state where the contact surface of the material does not move relative to the surface of the platen. τ (the shear stress on the contact surface owing to the pressure, μp) will not increase to a value higher than that necessary to produce yielding or plastic flow. When the value of τ increases to a level at which plastic flow is invoked, relative sliding between the platen and specimen surface stops (sticking occurs). Subsequently, *spreading action* of the specimen occurs owing to the *shear strain* of the surface layer, which creates a new contact surface with the platen at the radial end region (rollover occurs). In such a shear stress regime where the value of τ is high because the platen restrains the free sliding of the surface layer of the specimen, a condition approximating the hydrostatic pressure is developed; the magnitude of the hydrostatic pressure equals p, upon which value a shear stress τ is superimposed. Figure 1(*d*) schematically illustrates such a stress state.

The von Mises yield criterion in such a stress state (Fig. 1(*d*)) is

$$\frac{1}{\sqrt{2}}\sqrt{(\sigma_n-\sigma_r)^2+(\sigma_r-\sigma_c)^2+(\sigma_c-\sigma_n)^2} = \frac{1}{\sqrt{2}}\sqrt{(2\tau_o)^2+\tau_o^2+\tau_o^2} = \sigma_o \tag{6}$$

where τ_o is the maximum value of τ, which is the yield stress in pure shear. From Eq. (6), the relationship between σ_o and τ_o is established as

$$\tau_o = k\sigma_o \tag{7}$$

where $k = 1/\sqrt{3} = 0.57735$. Equation (7) is *the constant friction law* applied when shear yielding occurs. The relationship between the Coulomb friction law and the constant friction law is illustrated in Fig. 1(*b*).

The condition under which sticking occurs can be determined by considering the critical moment when τ ($=\mu p_c$) reaches τ_o ($=k\sigma_o$)

$$k\sigma_o = \mu p_c \tag{8}$$

where p_c is the critical pressure above which the law of constant friction is applied (Fig. 1(*b*)) and the shear stress reaches the level at which plastic flow is invoked (sticking occurs). As $p_c = k\sigma_o/\mu$, if μ reaches k, $p_c = \sigma_o$; the law of constant friction begins to be applied (sticking occurs) when the pressure (p) reaches the flow stress of the specimen (σ_o). In this regard, Schroeder and Webster considered that, if $\mu \geq k$, sticking occurs everywhere in the specimen.

Schroeder and Webster used Eq. (7), the law of constant friction, in considering the stress equilibrium of an axisymmetric stress element being compressed and established a differential equation:

$$dp = -\frac{2k\sigma_o}{H}dr \tag{9}$$

The profile of the pressure (p) for the sticking surface can be determined by integrating Eq. (8) from σ_o to p (the left side) and from R to r (the right side).

$$\frac{p}{\sigma_o} = 1 + \frac{2k}{H}(R-r) \tag{10}$$

Equation (10) is called the "SW-sticking profile of the pressure" in this study. An example of this profile is illustrated in Fig. 1(*a*) as curve "b". By substituting Eq. (10) into Eq. (4), the compensation model is obtained as

$$\frac{p_a}{\sigma_o} = 1 + \frac{k}{3}\frac{D}{H} \tag{11}$$

Equation (11) is called the "SW-sticking compensation model" in this study.

2.1.3 Mixed Surface. Schroeder and Webster considered that, even when $\mu \leq k$, sticking occurs on the surface portion when the pressure p is higher than its critical value p_c ($=k\sigma_o/\mu$); the equality $\tau = \tau_o = k\sigma_o$ (constant friction law) is applied in any region where $p > p_c$. As p is higher in the central region than at the radial end, the view that sticking occurs when $p > p_c$ yields the concept of the critical radius (r_c) below which sticking occurs and above which sliding occurs. The concepts of p_c and the associated r_c are illustrated in Fig. 2(*a*). When $r < r_c$, $p > p_c$, and thus, sticking occurs. When $r > r_c$, $p < p_c$, and thus, sliding occurs. We call this surface the *mixed contact surface* in that sticking and sliding occur simultaneously on a given contact surface. The value of r_c can be obtained by substituting $p_c = k\sigma_o/\mu$ for p in the pressure profile (Eq. (3); the sliding curve in Fig. 2(*a*)). The expression for r_c is

$$r_c = R - \frac{H}{2\mu}\ln\frac{k}{\mu} \tag{12}$$

The change in r_c with H is illustrated in Fig. 2(*b*) for a range of μ values.

The condition for the SW surface type, i.e., whether $p > p_c$ or $p < p_c$ when $\mu \leq k$, is graphically illustrated in Fig. 3(*a*). This surface-type map was established by observing the phenomenon of the mixed contact surface (the curves in Fig. 2(*a*)) from the ordinate (p).

If the phenomenon of the mixed contact surface (the curves in Fig. 2(*a*)) is observed from the abscissa (r), a different version of the surface-type map is established as follows. For the mixed surface, r_c should be positive. When $r_c = 0$, Eq. (12) transforms to

$$\left(\frac{H}{D}\right)_c = \frac{\mu}{\ln(k/\mu)} \tag{13}$$

When $(H/D) < (H/D)_c$, $r_c > 0$, and thus, a mixed surface is obtained. In contrast, when $(H/D) > (H/D)_c$, $r_c < 0$, and thus, the

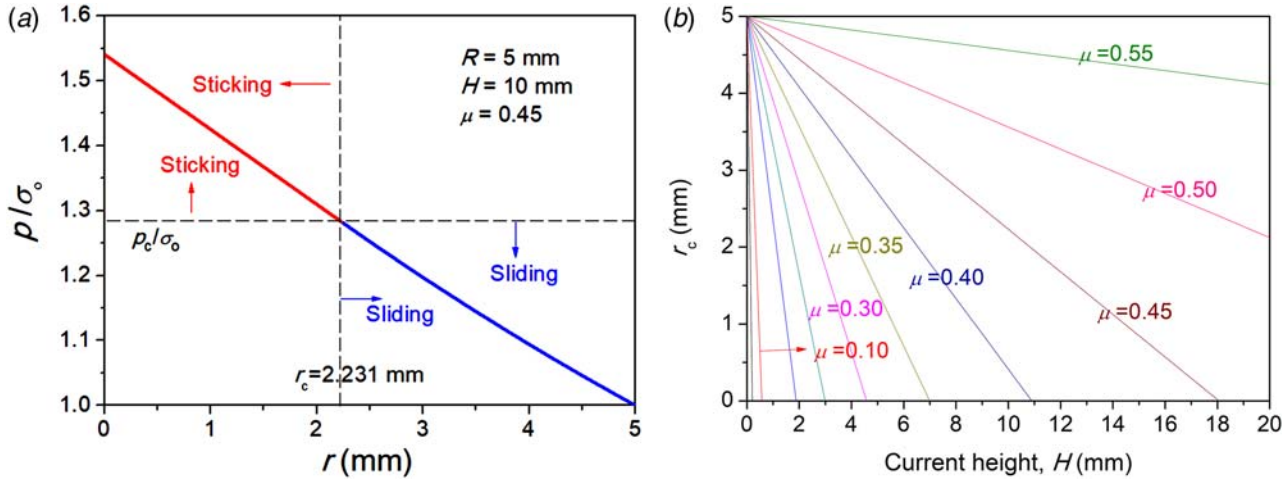

Fig. 2 (*a*) Example of the pressure profile on the mixed contact surface ($R = 5$ mm). r_c is the critical radius below which $p > p_c$, and thus, sticking occurs; p_c ($= k\sigma_o/\mu$) is the critical pressure above which sticking occurs. The sliding curve was drawn using Eq. (3) and the sticking curve using Eq. (14). (*b*) The change in the value of r_c as a function of H when $R = 5$ mm.

entire contact surface is sliding. The map of the surface type established using Eq. (13) is graphically illustrated in Fig. 3(*b*). The two versions of the surface-type map (Figs. 3(*a*) and 3(*b*)) are the same; they are obtained by observing the phenomenon of the mixed contact surface (the curves in Fig. 2(*a*)) from the ordinate (p) or from the abscissa (r), respectively.

The pressure profile (p) when $r < r_c$ can be determined by integrating Eq. (9) over the range $0 \le r \le r_c$, i.e., integration from p_c to p (the left side) and from r_c to r (the right side)

$$\frac{p}{\sigma_o} = \frac{p_c}{\sigma_o}\left(=\frac{k}{\mu}\right) + \frac{2k}{H}(r_c - r) \tag{14}$$

The pressure profile over the range $r_c \le r \le R$ is given by Eq. (3). The "SW-mixed pressure profile" is composed of two parts: Eq. (14) over the range $0 \le r \le r_c$ (e.g., the red curve in Fig. 2(*a*)) and Eq. (3) over the range $r_c \le r \le R$ (e.g., the sliding curve in Fig. 2(*a*)).

The compensation model for the mixed surface can be obtained by substituting Eq. (14) into Eq. (4) over the range $0 \le r \le r_c$ and substituting Eq. (3) into Eq. (4) over the range $r_c \le r \le R$ as follows:

$$\frac{p_a}{\sigma_o} = \frac{2}{\alpha^2}[(\beta+1)e^{\alpha-\beta} - \alpha - 1] + \frac{\beta^2}{\alpha^2}\left(\frac{k}{\mu} + \frac{2k}{3}\frac{r_c}{H}\right) \tag{15}$$

where α ($=2\mu R/H$) is the same as before and $\beta = 2\mu r_c/H$. Equation (15) is called the "SW-mixed compensation model" in this study.

2.2 Compensation Models for Sliding Surfaces. Schroeder and Webster derived the compensation models for each of the three types of contact surfaces. Other researchers developed their compensation models for the *sliding surface*. In this subsection, various compensation models of the sliding surface are reviewed in chronological order including the SW-sliding model.

As early as 1923, Siebel [22] derived the average additional stress (σ_{ra}) necessary to deform a 2D (plane strain) solid when uniform friction exists at the contact surfaces as follows:

$$\sigma_{ra} = \sigma_o \frac{\mu b}{2H} \tag{16}$$

where b is the current width and H is the current height of the work piece. As $\sigma_{ra} = p_a - \sigma_o$, Eq. (16) transforms to

$$\frac{p_a}{\sigma_o} = 1 + \frac{\mu b}{2H} \tag{17}$$

The compensation model of Siebel (Eq. (17)) is introduced here because, in the literature [11,24–26,39], the model of Hill (Eq. (18))

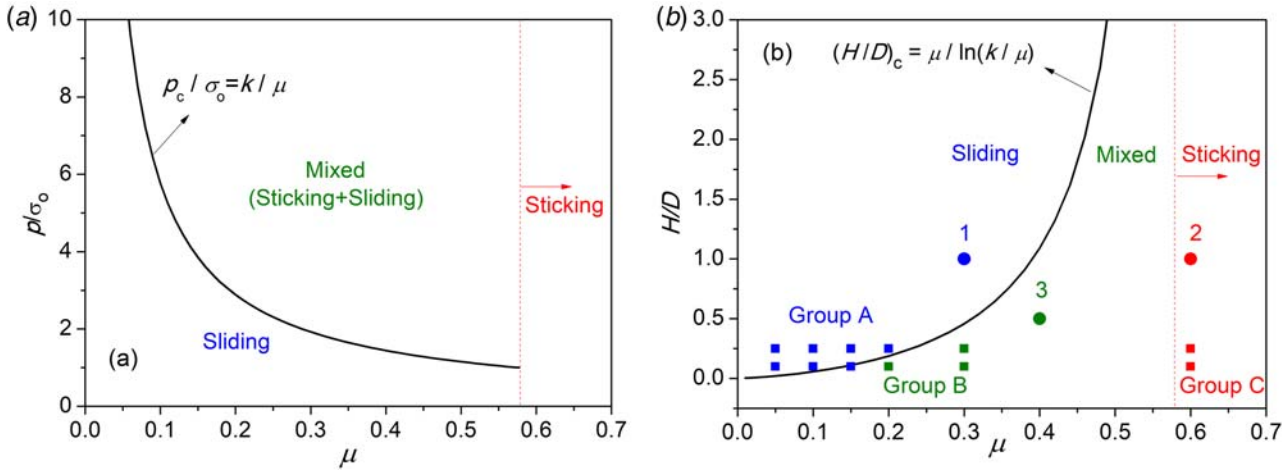

Fig. 3 Schematic illustration of the surface-type map. (*a*) The surface-type map from the viewpoint of the ordinate of Fig. 2(*a*): whether $p < p_c$ or $p > p_c$. (*b*) A different version of the surface-type map from the viewpoint of the abscissa of Fig. 2(*a*): whether $r_c > 0$ or $r_c < 0$. Closed circles labeled as 1, 2, and 3 are the conditions of the contact surfaces tested in this study. Closed squares indicate the conditions under which the pressure profiles and compensation models are examined in this study.

or even the SW-sliding model (Eq. (5)) is often referred to as Siebel's model [22,23]. However, Ref. [22] reported Eq. (17) only; Ref. [23] dealt with the axial compression of the specimen with a conically grooved surface.

In 1949, as already reviewed, Schroeder and Webster derived Eq. (5) (from Eqs. (3) and (4)) as the compensation model for a sliding surface. However, books [26,27] written later did not cite the study of Schroeder and Webster explicitly or introduce Eq. (5) as Siebel's model. Thus, some recent studies that used Eq. (5) [24,28] could not cite the study of Schroeder and Webster. To the best of our knowledge, Eqs. (3)–(5) were published first in the study of Schroeder and Webster. Han [24], Christiansen et al. [28], and Smith and Kassner [29] used Eq. (5) to compensate their quasi-static stress–strain curves. Altinbalik et al. [30] used the SW theory (Eq. (5)) to predict press loads in closed-die upsetting.

Hill [31] provided an approximate solution for Eqs. (3) and (4) in his book published in 1950 as follows:

$$\frac{p_a}{\sigma_o} = 1 + \frac{\mu D}{3H} \tag{18}$$

Richardson et al. [26] indicated that the error of Eq. (18) is less than 1% compared with that of Eq. (5) if $\mu D/H \leq 0.35$. Kamler et al. [39] used Eq. (18) to compensate their stress–strain curves measured using the split Hopkinson pressure bar.

In 1967, Rand [32] also presented a solution for Eqs. (3) and (4) as follows:

$$\frac{p_a}{\sigma_o} = \frac{\beta^2}{2(e^{\beta} - \beta - 1)} \quad \text{and} \quad \gamma = \frac{\mu D_o}{H_o(1+e)^{3/2}} \tag{19}$$

where D_o and H_o are the initial diameter and initial height, respectively, and e is the engineering strain. Bertholf and Karnes [40] used Eq. (19) to compensate their stress–strain curves obtained using the split Hopkinson pressure bar.

Cha et al. [41] considered the energy equilibrium of the cylinder specimen being compressed under sliding contact condition, from which a compensation model was derived as follows:

$$\frac{p_a}{\sigma_o} = \left(1 - \frac{\mu D}{3H}\right)^{-1} \tag{20}$$

They used Eq. (20) in correcting the stress–strain curves determined from split Hopkinson pressure bar signals.

3 Methods

To verify the "*three types of surfaces*" in the SW theory (marked as points 1, 2, and 3 in Fig. 3(*b*)), 2D axisymmetric finite element (FE) models with a radius of 5 mm and heights of 10, 10, and 5 mm, respectively, were constructed using axisymmetric four-node reduced integral elements (CAX4R). The length of the mesh was 31.25 μm in the radial direction and 100 μm in the axial direction. A separate mesh sensitivity test was performed carefully from the viewpoints of the radial displacement of the nodes and axial stress of the elements, both located at the top of the specimen. An example of the FE model will be presented later in Fig. 4(*c*). An elastic and perfectly plastic material model with an elastic modulus of 115 GPa and flow stress of 90 MPa (σ_o) was employed. The top and bottom platens were modeled using analytically rigid surfaces. Coulomb friction coefficients corresponding to points 1, 2, and 3 (Fig. 3(*b*)) were applied between the top/bottom platens and specimen surfaces. The displacement of the top platen was controlled to simulate the compression test. The pressure at the top elements of the specimen and radial displacement at the top nodes were obtained at a given axial strain of the specimen. A commercial FE package (ABAQUS), which employs the von Mises yield criterion, was used as the solver; plastic flow of the material occurs when the value of τ reaches $\tau_o(=k\sigma_o)$.

To verify the "*radial profile of the averaged pressure*" and the "*compensation models,*" various FE models with a radius of 5 mm were modeled according to the points marked as groups A, B, and C (Fig. 3(*b*)). The mesh density, modeling of platens, displacement control, and solver were the same as those mentioned above except that an elastic and work hardening material model was employed instead of the elastic–perfectly plastic model. The work hardening flow stress (σ_o) was modeled using the Voce hardening law [1]: $\sigma_o = A + B[1 - \exp(-C\varepsilon)]$, where $A = 96.044$ MPa, $B = 261.374$ MPa, and $C = 6.127$ (oxygen-free high thermal conductivity copper [49]). To construct the radial profile of the pressure, instead of obtaining axial stress values from the top elements of the specimen, the axial stress value of each element along the height direction was extracted at a given radial position and the extracted values were averaged. This averaged value at a given radial position was used to plot the *radial profile of the averaged pressure*. The measured flow stress in this numerical experiment (p_a) was determined by obtaining the reaction force at the top platen and subsequently dividing it by the current contact area, which was calculated from the current length based on the assumption of volume constancy of the specimen.

4 Results and Discussion

4.1 Verification of the Three Types of Schroeder–Webster Surfaces. The sliding surface condition indicated by point 1 ($H_o/D_o = 1.0$ and $\mu = 0.3$) in Fig. 3(*b*) is examined first. Whether sliding occurs under this condition can be judged from the "pressure profile" and "displacement" at the top of the specimen. The profile of the pressure at the top elements of the FE model is presented in Fig. 4(*a*). The profiles were obtained for a range of axial true strain values. Figure 4(*a*) also shows the value of $p_c(=k\sigma_o/\mu)$ indicated by the dashed horizontal line. As shown in Fig. 4(*a*), the value of the pressure is higher at the radial end than at the center, which contradicts the SW theory (Fig. 1(*a*)).

The radial displacement of top nodes is a more direct indicator of sliding than the pressure profile; it is presented in Fig. 4(*b*). The numbers of top nodes were assigned to increase from the center (node 1) to the radial end (node 11) at a constant interval in distance, which are marked in the left diagram of Fig. 4(*c*). Up to the axial strain value of approximately 0.1, which is the small-strain regime where the SW theory is anticipated to be valid, only node 11 expands significantly, whereas all other interior nodes are stationary. This finding contradicts the SW theory for the sliding surface, which anticipates the radial expansion of all nodes. As the axial strain increases to higher values, barreling and rollover of the side wall take place.

The *sticking surface* condition indicated by point 2 ($H_o/D_o = 1.0$ and $\mu = 0.6$) in Fig. 3(*b*) is examined next. The pressure profile at the top elements of the specimen is presented in Fig. 5(*a*). In Fig. 5(*a*), the pressure value on the top surface is generally higher at the radial end than at the center. Further, the pressure values are lower than the value of p_c at the central region up to the axial strain value of 0.357. These observations contradict the SW theory for the sticking surface, which predicts (1) higher pressure at the center than at the radial end and (2) $p > p_c$ over the entire contact surface.

The radial displacement of the top nodes of the specimen is presented in Fig. 5(*b*). As can be seen in Fig. 5(*b*), all nodes except for the center node expands radially. This finding also contradicts the SW-sticking theory, which anticipates sticking (no sliding) of all nodes.

Finally, the mixed surface condition indicated by point 3 ($H_o/D_o = 0.5$ and $\mu = 0.4$) in Fig. 3(*b*) is examined. The profile of the pressure at the top elements of the specimen is presented in Fig. 6(*a*). When the value of the axial strain is small, e.g., 0.105, the pressure profile is lower than the value of p_c up to the radial end, which also contradicts the SW theory for the mixed surface, which anticipates a profile similar to the one in Fig. 2(*a*): p values should be higher than the p_c value in the central region.

The radial displacement of the top nodes of the specimen is presented in Fig. 6(*b*) as a function of the axial true strain. Nodes 7–11

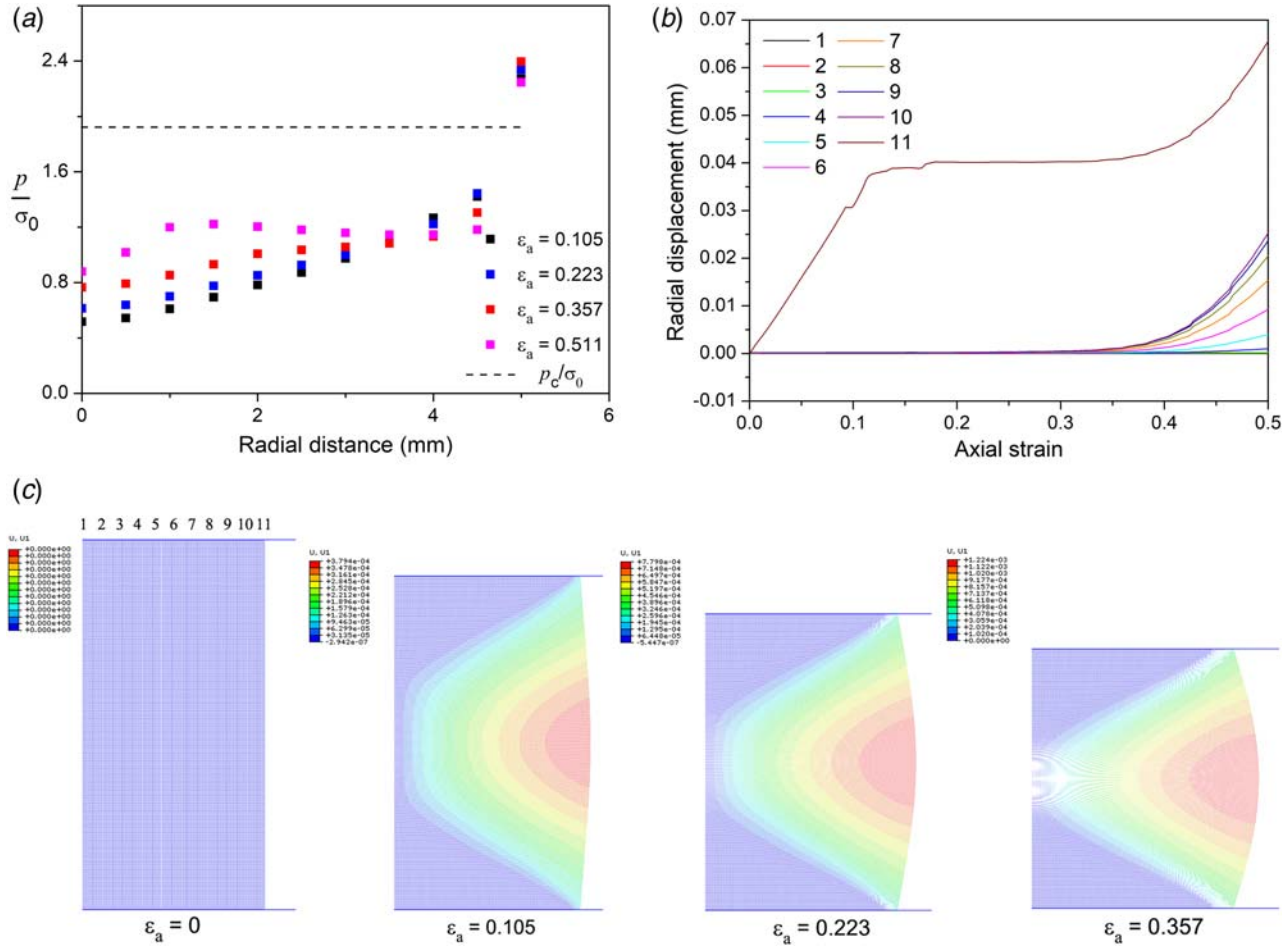

Fig. 4 Result of simulation under the sliding surface condition marked as 1 ($H_o/D_o = 1.0$ and $\mu = 0.3$) in Fig. 3(*b*). (*a*) Radial profile of the pressure on the top elements of the specimen. The radial position is based on the undeformed shape of the specimen. (*b*) Radial displacements of the top nodes as a function of the axial true strain. (*c*) Deformed shapes of the specimen with radial displacement contour (U1: axial displacement).

at the annular zone near the radial end move to the positive direction, whereas nodes 1–6 in the central region are almost stationary. Purely judging from node displacement, the SW-mixed surface seems to be manifested. However, note that such movement of nodes occurred at a small strain value (0.105) when the pressure value was lower than the value of p_c up to the radial end (Fig. 6(*a*)). Overall, the SW theory for the mixed surface is not manifested.

As mentioned, the contact surfaces of the SW theory were predicted from the two fundamental assumptions that (i) there is no barreling and (ii) inclusion of the frictional force does not alter

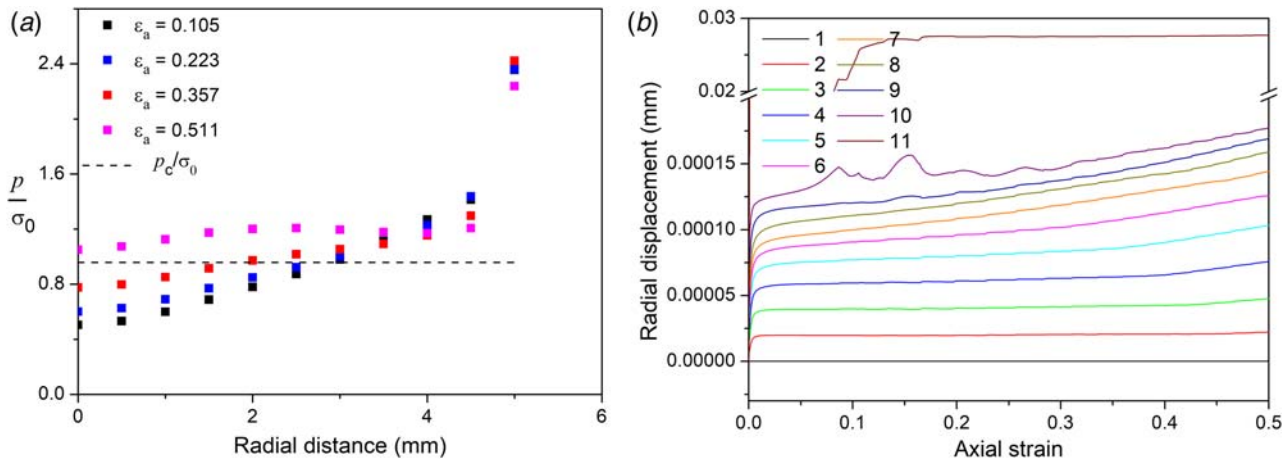

Fig. 5 Result of simulation under the sticking surface condition marked as 2 ($H_o/D_o = 1.0$ and $\mu = 0.6$) in Fig. 3(*b*). (*a*) Radial profile of the pressure on the top elements of the specimen. The radial position is based on the undeformed shape of the specimen. (*b*) Radial displacements of the top nodes as a function of the axial true strain.

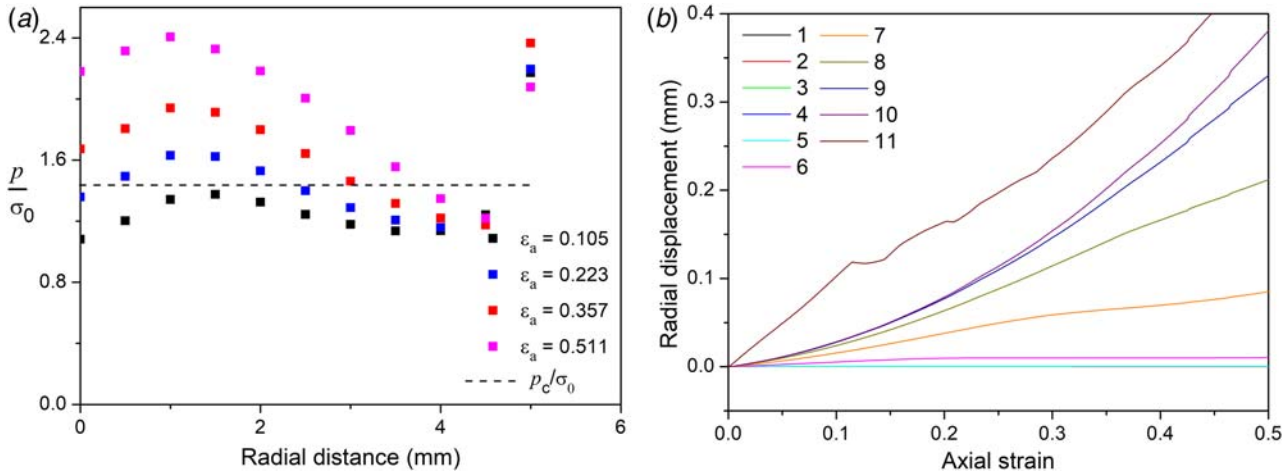

Fig. 6 Result of simulation under the sticking surface condition marked as 3 ($H_o/D_o = 0.5$ and $\mu = 0.4$) in Fig. 3(*b*). (*a*) Radial profile of the pressure on the top elements of the specimen. The radial position is based on the undeformed shape of the specimen. (*b*) Radial displacements of the top nodes as a function of the axial true strain.

the stress state of the specimen. Absence of barreling inherently indicates the statement described by Thompsen et al. [27]: "The slab method of solution assumes that stresses on a plane or spherical surface are perpendicular to the flow direction. The stresses are not permitted to vary on this plane. A slab, straight or curved, of infinitesimal thickness is selected parallel to this plane at any arbitrary point in the deformed metal". From the force balance of the slab, the basic differential models such as Eqs. (2) and (9) were derived. However, barreling and rollover of the specimen occur during plastic deformation, as shown in Fig. 4(*c*). Further, the inclusion of the frictional force should alter the stress state of the specimen. Violation of the two fundamental assumptions as such is believed to be the reason the three types of contact surfaces of the SW theory are not manifested in the numerical simulation.

4.2 Verification of the Radial Profile of Pressure. The three types of SW compensation models were obtained by applying the pressure profile along the radial direction (Eq. (3) for the sliding surface, Eq. (10) for the sticking surface, and Eqs. (14) and (3) for the mixed surface) to Eq. (4). Therefore, the pressure profiles (Eqs. (3), (10), and (14)) directly govern the reliability of the compensation models. In this regard, the radial profiles of the pressure are numerically verified first in this subsection, followed by the compensation models in Sec. 4.3.

As the three types of SW contact surfaces (sliding, mixed, and sticking surfaces) are not manifested in the numerical simulation, the pressure profiles for sticking and sliding surfaces are compared together, regardless of the H/D and μ conditions. When the H/D and μ conditions belong to the mixed-surface regime (Fig. 3(*b*)), profiles derived for the mixed surface are also compared.

In this study, the *averaged* value of the pressure of the elements *along the height direction* of the barreled specimen was obtained. This averaged pressure along the height direction is presented as a function of the radial position (instead of the radial profile using the pressure of elements only at the top of the specimen). The reason the averaged pressure along the height direction is used is because the value of p_a (the stress of the specimen measured using the load cell in the experiment) appearing in the compensation model results from all of the specimen volume from top to bottom. The example of the radial profile of the averaged pressure is presented in Fig. 7(*a*) as the curve in black for a condition ($H/D = 0.25$ and $\mu = 0.15$) belonging to group A (the sliding surface) in Fig. 3(*b*). Figure 7(*a*) also shows the SW-sliding and SW-sticking pressure profiles.

In Fig. 7(*a*), unlike the pressure profile at the top surface of the specimen (see Fig. 4(*a*)), the *averaged* pressure profile is higher at the center of the specimen than at the radial end. Interestingly, the SW-sliding profile is remarkably consistent with the profile of the averaged pressure of the barreled specimen (obtained via the numerical experiment). Although the three types of contact surfaces are not manifested at the top of the specimen, the SW-sliding pressure profile (Eq. (3)) reasonably describes the averaged pressure profile of the barreled specimen. The reliability of the SW-sliding compensation model (Eq. (5)) in consequence of this phenomenon is discussed in Sec. 4.3.

Figure 7(*b*) compares the profiles of the averaged pressure for a contact condition ($H/D = 0.25$ and $\mu = 0.3$) belonging to group B (the mixed surface) in Fig. 3(*b*). Figure 7(*b*) also shows the SW profiles for sliding, mixed, and sticking surfaces. For the considered case, the SW-mixed pressure profile (Eq. (14) plus Eq. (3)) is the best; it describes the averaged pressure profile reasonably.

Figure 7(*c*) compares the profiles of averaged pressure for a condition ($H/D = 0.25$ and $\mu = 0.6$) belonging to group C (the sticking surface) in Fig. 3(*b*). Figure 7(*c*) also shows the SW profiles for sliding and sticking surfaces. For the considered case ($H_o/D_o = 0.25$ and $\mu = 0.6$), the SW-sticking profile is better than the SW-sliding profile while the former describes the averaged pressure profile only roughly.

4.3 Verification of Friction Compensation Models. The SW compensation models developed for the three types of contact surfaces and other models are verified here. The compensation models for the sliding surface is examined first. Figure 10 presents the stress–strain curves measured in the numerical experiment (solid curves) for specimens with H_o/D_o ratios of 0.25 and 0.10 (fairly thin specimens). These thin specimens have an advantage in examining the compensation models in a rigorous manner because the amount of friction compensation is higher for a specimen with lower H/D than for a specimen with higher H/D; the influence of friction on the stress state of the specimen is also augmented. The considered conditions of H/D and μ belong to group A (Fig. 3(*b*)) except when $\mu = 0.2$ and $H/D = 0.1$ (this condition belongs to group B).

In Fig. 8, the solid curve for $\mu = 0$ is the measured p_a curve in the numerical experiment when the Coulomb friction coefficient is zero. This measured curve is the same as the input property of the specimen (σ_o) for the numerical experiment. This consistency indicates the reliability of the current numerical experiment. As the value of μ increases, the stress–strain curve measured in the numerical experiment (the solid curve) is shifted upward (overestimated), as anticipated. In Fig. 8, all the considered specimens except when

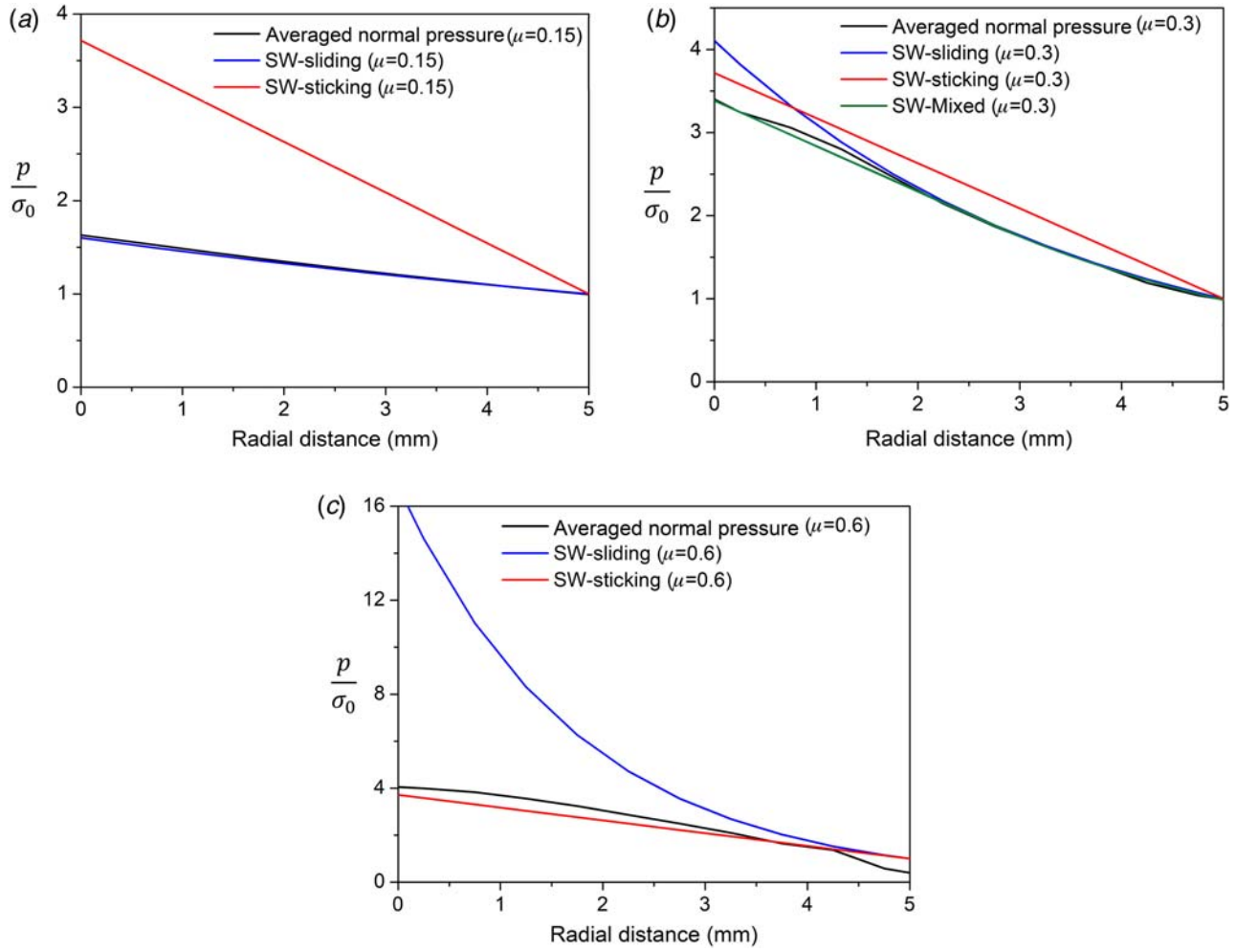

Fig. 7 Profiles of the averaged pressure and SW profiles when the axial strain is 0.16 for the cases when $H_o/D_o = 0.25$ and (*a*) $\mu = 0.15$, (*b*) $\mu = 0.30$, and (c) $\mu = 0.60$, which correspond to the nominal contact conditions for sliding (group A), mixed (group B), and sticking (group C) surfaces, respectively. The radial position is based on the undeformed shape of the specimen.

$\mu = 0$ exhibits significant barreling (not shown) similar to the specimen presented in Fig. 4(*c*).

Figure 8 also shows the stress–strain curves (dashed curves) predicted using various compensation models developed for the sliding surface: the models of Rand [32], Hill [31], Cha et al. [41], and SW-sliding [21]. The dashed curves were constructed by multiplying the solid curve when $\mu = 0 (\sigma_0)$ by the ratio of p_a/σ_o (the friction compensation model).

In Fig. 8, the dashed curve when $\mu = 0.2$ and $H_o/D_o = 0.1$ (a mixed-surface condition; see Fig. 3(*b*)) is added as a comparison curve to show how the compensation models developed for the sliding surface (the dashed curves) work for the specimen under the mixed-surface condition. It is observed in Fig. 8 that, if the condition in terms of μ and H_o/D_o belongs to the sliding surface (up to the μ value of 0.15; group A), the SW-sliding model is remarkably capable in predicting the stress–strain curve of the barreled specimen (solid curves) down to the H_o/D_o ratio of 0.1; it is observed to be the best among the considered models.

As mentioned, the sliding contact surface itself is not manifested in the numerical simulation. Such remarkable consistency of the SW-sliding model to the curves measured in the numerical experiment is achieved because the SW-sliding profile of the pressure (Eq. (3)) could describe the averaged pressure profile of the barreled specimen reasonably well (Fig. 7(*a*)). Therefore, if the condition in terms of μ and H_o/D_o of the specimen belongs to the sliding surface regime (Fig. 3(*b*)), it is desirable to use the SW-sliding compensation model.

The reliability of the compensation model developed for the mixed surface is examined next. Figure 9 depicts the stress–strain curves measured in the numerical experiment (solid curves) for barreled specimens under the conditions belonging to group B (Fig. 3(*b*)). As shown in Fig. 9(*a*) ($H_o/D_o = 0.1$ and $\mu = 0.1$), the prediction capability of the SW-mixed model is remarkable. However, in Fig. 9(*b*) ($H_o/D_o = 0.1$ and $\mu = 0.3$), the SW-sticking model is unexpectedly better than the SW-mixed model; the former predicts p_a values (solid curve) reasonably well while the SW-mixed model describes only roughly. For the case of Fig. 9(*c*) ($H_o/D_o = 0.1$ and $\mu = 0.3$), although the SW-mixed model is the best, it fails to predict p_a values (solid curve) reasonably (describes only roughly). Overall, the prediction capability of the SW-mixed model is inferior to that of the SW-sliding model for specimens in the sliding-surface regime (Fig. 8). If the H_o/D_o ratio and μ conditions belonging to the mixed-surface regime (Fig. 3(*b*)) are unavoidable, there is no other choice but to use the SW-mixed model for friction compensation by admitting the fact that the prediction capability of the SW-mixed model in such a case is inferior to that of the SW-sliding model for specimens in the sliding surface regime.

Finally, the reliability of the compensation model developed for the sticking surface is examined. Figure 10 presents the stress–strain curves measured in the numerical experiment (solid curves) for specimens when the H_o/D_o and μ condition is in the sticking-surface regimen (group C in Fig. 3(*b*)). In the considered cases, the SW-sticking model is superior to the SW-sliding model.

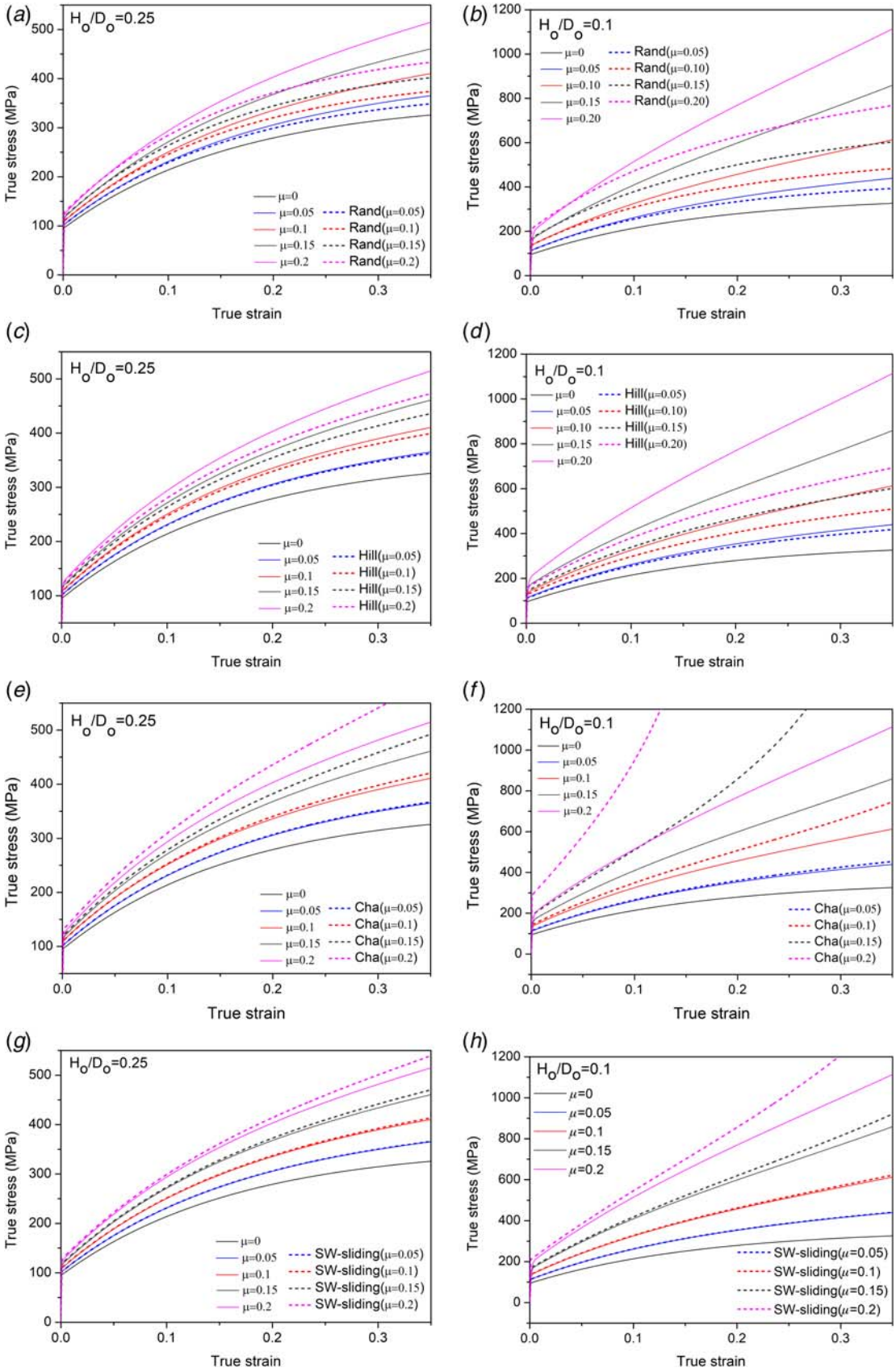

Fig. 8 Stress–strain curves (solid) measured in the numerical experiment and the curves (dashed) predicted using the compensation models when H_o/D_o and μ conditions are in the *sliding-surface regime (group A)* in Fig. 3(*b*) except for the case when $\mu = 0.2$ and $H_o/D_o = 0.1$ (group B). (*a*) and (*b*) are for the model of Rand, (*c*) and (*d*) are for the model of Hill, (*e*) and (*f*) are for the model of Cha et al. [41], and (*g*) and (*h*) are for the SW-sliding model.

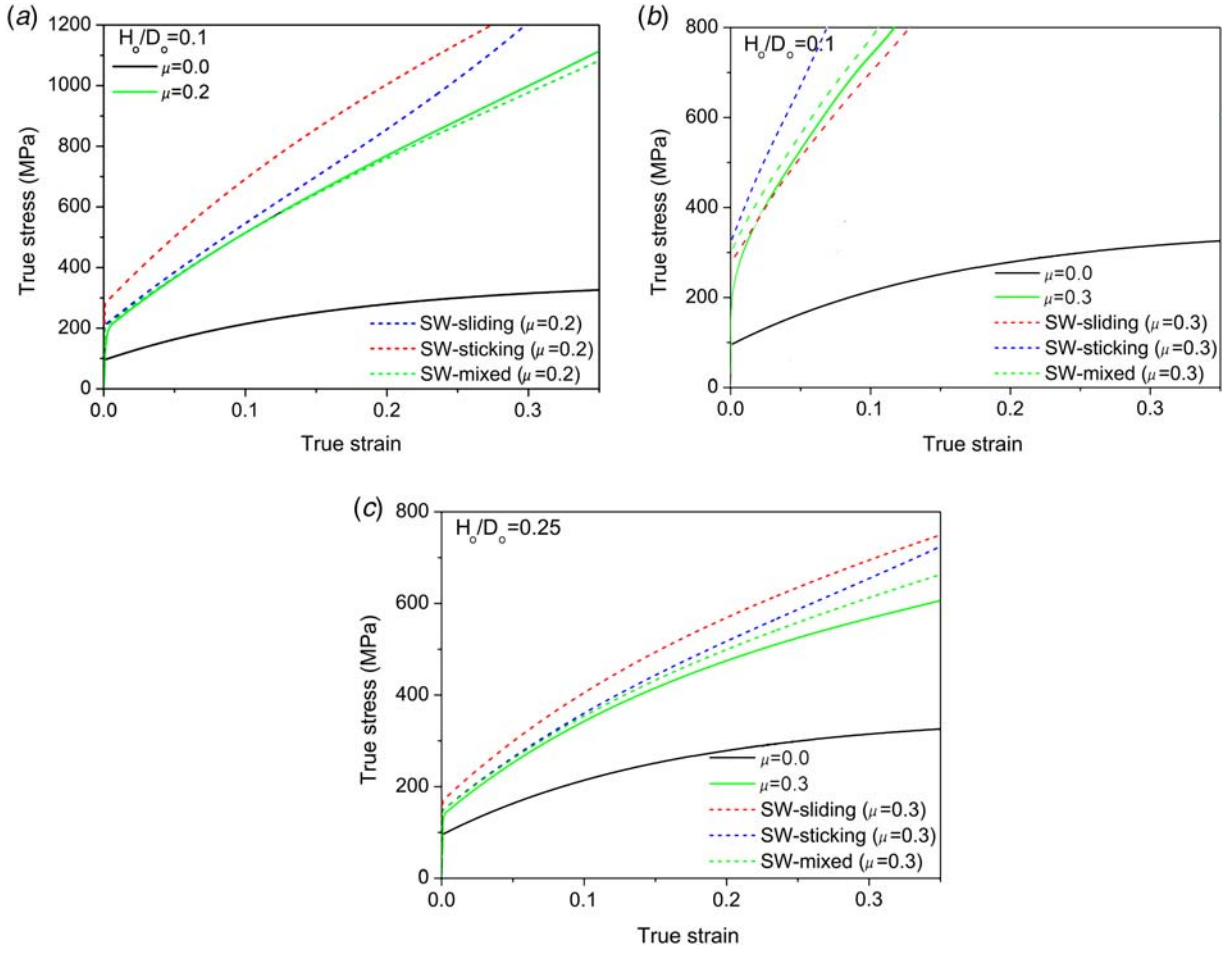

Fig. 9 Stress–strain curves (solid) measured in the numerical experiment and the curves (dashed) predicted using the compensation models when H_o/D_o and μ conditions are in the *mixed-surface regime (group B)* in Fig. 3(*b*). The H_o/D_o and μ values are (*a*) 0.1 and 0.2, (*b*) 0.1 and 0.3, and (*c*) 0.25 and 0.3, respectively.

However, the prediction capability of the SW-sticking model is inferior to that of the SW-sliding compensation model for specimens in the sliding-surface regime (Fig. 8). If the H_o/D_o ratio and μ conditions belonging to sticking-surface regime (Fig. 3(*b*)) are unavoidable, there is no other choice but to use the SW-sticking model for friction compensation by admitting the fact that the prediction capability of the SW-sticking model in such a case is inferior to that of the SW-sliding model for specimens in the sliding surface regime.

4.4 Further Discussions. In the literature, compensation models developed for the sliding surface have been generally used to compensate for the measured stress–strain curve because the curve is usually measured under a lubricated condition. If the

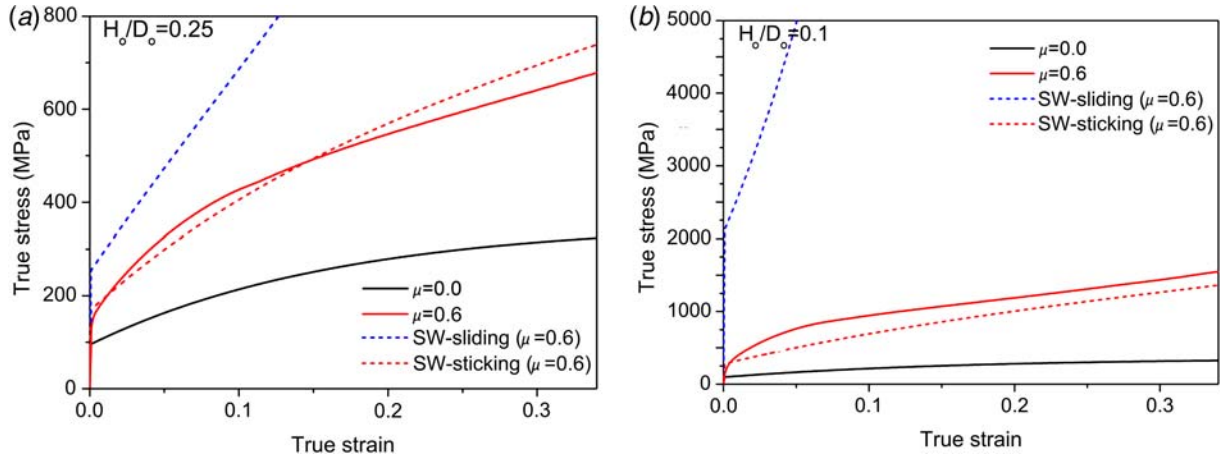

Fig. 10 Stress–strain curves (solid) measured in the numerical experiment and the curves (dashed) predicted using the compensation models when the H_o/D_o and μ conditions are in the *sticking-surface regime (group C)* in Fig. 3(*b*). The H_o/D_o and μ values are (*a*) 0.25 and 0.6 and (*b*) 0.1 and 0.6, respectively.

H/D ratio of the specimen is not very low, the magnitude of compensation itself is small regardless of the type of the compensation model used. Consequently, the difference resulting from the choice of the compensation model is also diminished.

All the SW compensation models for the sliding, mixed, and sticking surfaces consider the plastic flow of the specimen under axisymmetric compression. However, only the SW-sliding compensation model demonstrates remarkable capability in predicting the flow stress of the barreled specimen (Fig. 8) because the SW-sliding profile of the pressure describes the averaged pressure profile of the barreled specimen reasonably well (Fig. 7(*a*)).

Therefore, for thin plate specimens in a quasistatic test or a low-*H/D* specimen in a high-strain-rate test such as the split Hopkinson bar test [18], direct impact test [19], and plate impact test [20], it is recommended to use the SW-sliding model for compensating the obtained stress–strain curve. In such a case, it is important to maintain the μ (and *H/D*) condition in the sliding regime (Fig. 3(*c*)) via lubrication.

5 Conclusions

In the SW theory, there are three types of contact surfaces, i.e., sliding, mixed, and sticking surfaces, depending on the *H/D* ratio of the specimen and μ. The *H/D* and μ conditions for each type of contact surface have been examined in this study via numerical simulation (FE analysis). Judging from (i) the radial profile of the pressure at the top elements of the specimen and (ii) the radial displacement at the top nodes, it is concluded that the three types of contact surfaces are not manifested in the numerical simulation.

Nevertheless, when the specimen is under an *H/D* and μ condition for the sliding surface, the SW-sliding compensation model is remarkably reliable in predicting the measured stress–strain curve of the barreled specimen in the numerical experiment down to the initial *H/D* ratio of 0.1; the SW-sliding model is the best among the compared models of Rand, Hill, and Cha et al. This result originates from the fact that the pressure profile of the SW theory for the sliding surface describes the averaged pressure profile of the barreled specimen reasonably well.

If the H_o/D_o ratio and μ conditions belonging to the mixed-surface regime or sticking-surface regimen (Fig. 3(*b*)) are unavoidable, there is no other choice but to use the SW-mixed model or SW-sticking model, respectively, for friction compensation by admitting the fact that the prediction capability of the SW-mixed model and SW-sticking model is inferior to that of the SW-sliding model for specimens in the sliding surface regime.

Therefore, it is important to maintain the μ (and *H/D*) condition in the sliding regime illustrated in Fig. 3(*c*) via lubrication. Then, it is recommended to use the SW-sliding model (among other models developed for the sliding surface) for compensating the experimentally obtained stress–strain curve.

Funding Data

- Defense Acquisition Program Administration (Korea) (Grant No. UC160008D; Funder ID: 10.13039/501100003626) through Poongsan Co.
- National Research Foundation of Korea (Grant No. 2017R1A6A3A11032774; Funder ID: 10.13039/501100003725).

Nomenclature

k = constant ($=1/\sqrt{3}=0.57735$)
p = pressure (axial stress) on the contact surface, Pa
r = radial position in the cylinder specimen, m
A = current cross-sectional area of the specimen, m
D = current diameter of the specimen, m
H = current height of the specimen, m
R = initial radius of the cylinder specimen, m
p_a = average pressure (stress) on the contact surface. Measured stress of the specimen under the presence of friction, Pa
p_c = critical pressure (stress) above which the phenomenon of sticking occurs, Pa
r_c = critical radius below which $p > p_c$, and thus, sticking occurs, m
D_o = initial diameter of the specimen, m
H_o = initial height of the specimen, m
ε_a = axial true strain
μ = coefficient in the Coulomb Friction law
σ_o = flow stress of the specimen. Friction-free stress of the specimen (true material property), Pa
σ_c = circumferential stress of the axisymmetric stress element, Pa
σ_n = stress of the axisymmetric stress element, Pa
σ_r = radial stress of the axisymmetric stress element, Pa
τ = frictional shear stress on the contact surface, Pa
τ_o = maximum frictional shear stress (flow stress in pure shear), Pa

References

[1] Voce, E., 1948, "The Relationship Between Stress and Strain for Homogeneous Deformation," J. Inst. Metals, **74**, pp. 537–562.
[2] Johnson, G. R., and Cook, W. H., 1983, "A Constitutive Model and Data for Metals Subjected to Large Strains, High Strain Rates and High Temperatures," Proceedings of the 7th International Symposium on Ballistics, Organizing Committee of the 7th ISB, Hague, Apr. 19–21, pp. 541–547.
[3] Shin, H., and Kim, J.-B., 2010, "A Phenomenological Constitutive Equation to Describe Various Flow Stress Behaviors of Materials in Wide Strain Rate and Temperature Regimes," ASME J. Eng. Mater. Technol., **132**(2), p. 021009.
[4] Nakamura, T., Tanaka, S., Hayakawa, K., and Fukai, Y., 2000, "A Study of the Lubrication Behavior of Solid Lubricants in the Upsetting Process," ASME J. Tribol., **122**(4), pp. 803–808.
[5] Azushima, A., 2000, "FEM Analysis of Hydrostatic Pressure Generated Within Lubricant Entrapped Into Pocket on Workpiece Surface in Upsetting Process," ASME J. Tribol., **122**(4), pp. 822–827.
[6] Azushima, A., Yanagida, A., and Tani, S., 2010, "Permeation of Lubricant Trapped Within Pocket Into Real Contact Area on the End Surface of Cylinder," ASME J. Tribol., **133**(1), p. 011501.
[7] Mizuno, T., and Hasegawa, K., 1982, "Effects of Die Surface Roughness on Lubricating Conditions in the Sheet Metal Compression-Friction Test," ASME J. Lubr. Technol., **104**(1), pp. 23–28.
[8] Ramaraj, T. C., and Shaw, M. C., 1985, "A New Method of Evaluating Metal-Working Lubricants," ASME J. Tribol., **107**(2), pp. 216–219.
[9] Krishna, C. H., Davidson, M. J., Nagaraju, C., and Kumar, P. R., 2015, "Effect of Lubrication in Cold Upsetting Using Experimental and Finite Element Modeling," J. Test. Eval., **43**(1), pp. 53–61.
[10] Misirili, C., 2014, "On Materials Flow Using Different Lubricants in Upsetting Process," Ind. Lub. Tribol., **66**(5), pp. 623–631.
[11] Banerjee, J. K., 1985, "Barreling of Solid Cylinders Under Axial Compression," ASME J. Eng. Mater. Technol., **107**(2), pp. 138–144.
[12] Banerjee, J. K., and Cárdenas, G., 1985, "Numerical Analysis on the Barreling of Solid Cylinders Under Axisymmetric Compression," ASME J. Eng. Mater. Technol., **107**(2), pp. 145–147.
[13] Lee, J.-H., Shin, H., Kim, J.-B., Kim, J.-Y., Park, S.-T., Kim, G.-L., and Yoon, T.-S., 2019, "Determination of the Flow Stress–Strain Curve of Aluminum Alloy and Tantalum Using Compressive Load–Displacement Curves of a Hat-Type Specimen," ASME J. Appl. Mech., **86**(3), p. 031012.
[14] Lee, C. H., and Altan, T., 1972, "Influence of Flow Stress and Friction Upon Metal Flow in Upset Forging of Rings and Cylinders," J. Eng. Ind., **94**(3), pp. 775–782.
[15] Kim, S.-H., Kim, M.-K., Shin, H., and Lee, K. Y., 2018, "Measurement of a Nearly Friction-Free Stress–Strain Curve of Silicone Rubber up to a Large Strain in Compression Testing," Exp. Mech., **58**(9), pp. 1479–1484.
[16] Tan, X., 2011, "Evaluation of Friction in Upsetting," Prod. Eng. Res. Dev., **5**(2), pp. 141–149.
[17] Lee, J.-H., Shin, H., Seo, S.-J., Lee, J.-G., Lee, J.-O., Yoon, T.-S., and Jeong, C.-S., 2019, "A Design of a Phenomenological Friction-Compensation Model via Numerical Experiment for the Compressive Flow Stress–Strain Curve of Copper (in Korean)," Kor. J. Comput. Design Eng., **24**(1), pp. 1–9.
[18] Shin, H., and Kim, J.-B., 2019, "Evolution of Specimen Strain Rate in Split Hopkinson Bar Test," Proc. Inst. Mech. Eng. C, **233**(13), pp. 4667–4687.
[19] Couque, H., 2014, "The Use of the Direct Impact Hopkinson Pressure Bar Technique to Describe Thermally Activated and Viscous Regimes of Metallic Materials," Philos. Trans. R. Soc. A, **372**, p. 20130218.
[20] Frutschy, K. J., and Clifton, R. J., 1998, "High-Temperature Pressure-Shear Plate Impact Experiments on OFHC Copper," J. Mech. Phys. Sol., **46**(10), pp. 1723–1743.
[21] Schroeder, W., and Webster, D. A., 1949, "Press-Forging Thin Sections: Effect of Friction, Area, and Thickness on Pressure Required," ASME J. Appl. Mech., **16**, pp. 289–294.
[22] Siebel, E., 1923, "Grundlagen zur Berechnung des Kraft- und Arbeitsbedarfs Beim Schmieden und Walzen (Basics for Calculating the Force and Work Requirements of Forging and Rolling)," Stahl. Und. Eisen, **43**(41), pp. 1295–1298.
[23] Siebel, E., and Pomp, A., 1927, "Die Ermittlung der Formänderungsfestigkeit von Metallen Durch den Stauchversuch (Determination of the Deformation Strength

of Metals by the Compression Test),” Mitt. Kaiser. Wilhelm. Inst. Eisenforsch, **9**(8), pp. 157–171.
[24] Han, H., 2002, “The Validity of Mechanical Models Evaluated by Two-Specimen Method Under the Known Coefficient of Friction and Flow Stress,” J. Mater. Process. Technol., **122**(2–3), pp. 386–396.
[25] Loizou, N., and Sims, R. B., 1953, “The Yield Stress of Pure Lead in Compression,” J. Mech. Phys. Solids, **1**(4), pp. 234–243.
[26] Richardson, G. R., Hawkins, D. N., and Sellars, C. M., 1985, *Worked Examples in Metal Working*, Institute of Metals, London.
[27] Thompsen, E. G., Yang, C. T., and Kobayashi, S., 1965, *Mechanics of Plastic Deformation in Metal Processing*, Macmillan, New York.
[28] Christiansen, P., Martins, P. A. F., and Bay, N., 2016, “Friction Compensation in the Upsetting of Cylindrical Test Specimens,” Exp. Mech., **56**(7), pp. 1271–1279.
[29] Smith, K. K., and Kassner, M. E., 2016, “Through-Thickness Compression Testing of Commercially Pure (Grade II) Titanium Thin Sheet to Large Strains,” J. Metall., **2016**, p. 6178790.
[30] Altinbalik, T., Akata, H., and Can, Y., 2007, “An Approach for Calculation of Press Loads in Closed-Die Upsetting of Gear Blanks of Gear Pumps,” Mater. Des., **28**(2), pp. 730–734.
[31] Hill, R., 1950, *The Mathematical Theory of Plasticity*, Oxford University Press, London, pp. 262–281.
[32] Rand, J. L., 1967, *An Analysis of the Split Hopkinson Pressure Bar*, Technical Report (NOLTR 67-156), US Naval Ordnance Laboratory, Silver Spring, MD.
[33] Cook, M., and Larke, E. C., 1945, “Resistance of Copper and Copper Alloys to Homogeneous Deformation in Compression,” J. Inst. Metals, **71**(12), pp. 371–390.
[34] Avitzur, B., 1968, *Metal Forming: Processes and Analysis*, McGraw-Hill, New York.
[35] Schey, J. A., Venner, T. R., and Takomana, S. L., 1982, “The Effect of Friction on Pressure in Upsetting at Low Diameter-to-Height Ratios,” J. Mech. Work. Technol., **6**(1), pp. 23–33.
[36] Hartley, P., Sturgess, C. E. N., and Rowe, G. W., 1980, “Influence of Friction on the Prediction of Forces, Pressure Distributions and Properties in Upset Forging,” Int. J. Mech. Sci., **22**(12), pp. 743–753.
[37] Bugini, A., Maccarini, G., Giardini, C., Pacagnella, R., and Levi, R., 1993, “The Evaluation of Flow Stress and Friction in Upsetting of Rings and Cylinders,” CIRP Ann., **42**(1), pp. 335–338.
[38] Tan, X., Zhang, W., and Bay, N., 1999, “A New Friction Test Using Simple Upsetting and Flow Analysis,” Adv. Technol. Plast., **1**(6), pp. 365–370.
[39] Kamler, F., Niessen, P., and Pick, R. J., 1995, “Measurement of the Behaviour of High Purity Copper at Very High Rates of Straining,” Canad. J. Phys., **73**(5–6), pp. 295–303.
[40] Bertholf, L. D., and Karnes, C. H., 1975, “Two-Dimensional Analysis of the Split Hopkinson Pressure Bar System,” J. Mech. Phys. Solids, **23**(1), pp. 1–19.
[41] Cha, S. H., Shin, H., and Kim, J. B., 2010, “Numerical Investigation of Frictional Effects and Compensation of Frictional Effects in Split Hopkinson Pressure Bar (SHPB) Test (in Korean),” Trans. Korean Soc. Mech. Eng. A., **34**(5), pp. 511–518.
[42] Gorham, D. A., Pope, P. H., and Cox, O., 1984, “Sources of Error in Very High Strain Rate Compression Tests,” Inst. Phys. Conf. Ser., **1984**(70), pp. 151–158.
[43] Hall, I. W., and Guden, M., 2003, “Split Hopkinson Pressure Bar Compression Testing of an Aluminum Alloy: Effect of Lubricant Type,” J. Mater. Sci., **22**(21), pp. 1533–1535.
[44] Mori, L. F., Krishnan, N., Cao, J., and Espinosa, H. D., 2007, “Study of the Size Effects and Friction Conditions in Microextrusion—Part II: Size Effect in Dynamic Friction for Brass-Steel Pairs,” ASME J. Manuf. Sci. Eng., **129**(4), pp. 677–689.
[45] Wang, Z. J., and Cheng, L. D., 2009, “Experimental Research and Numerical Simulation of Dynamic Cylinder Upsetting,” Mater. Sci. Eng., **499**(1–2), pp. 138–141.
[46] Jankowiak, T., Rusinek, A., and Lodygowski, T., 2011, “Validation of the Klepaczko–Malinowski Model for Friction Correction and Recommendations on Split Hopkinson Pressure Bar,” Finite Elem. Anal. Des., **47**(10), pp. 1191–1208.
[47] Lu, Y., and Zhang, S., 2013, “Study on Interface Friction Model for Engineering Materials Testing in Split Hopkinson Pressure Bar Tests,” Mod. Mech. Eng., **3**(1), pp. 27–33.
[48] Siviour, C. R., and Walley, S. M., 2018, “Inertial and Frictional Effects in Dynamic Compression Testing,” *The Kosky-Hopkinson Bar Machine*, Springer, New York, pp. 205–247.
[49] Shin H., and Kim, J.-B., 2012, “Description Capability of a Simple Phenomenological Model for Flow Stress of Copper in an Extended Strain Rate Regime,” Proceedings of the 4th International Conference on Design and Analysis of Protective Structures, Jeju, Korea, June 19–22, Paper No. T8-10, pp. 1–6.